Magnetic Materials and System-Level Evaluation of RE-free Fe_2Ni_2N versus N35 Magnets under Inverter Voltage–Current Constraints in the 2012 Nissan Leaf IPMSM

Sayem Ul Alam[1], Shuhui Li[2], Yang-Ki Hong[3], Zhenghao Liu[4], Md Imtiaz Kamrul[5]
Department of Electrical and Computer Engineering
The University of Alabama
Tuscaloosa, Alabama 35487, USA
[1]salam7@crimson.ua.edu, [2]sli@eng.ua.edu, [3]ykhong@eng.ua.edu, [4]zliu99@crimson.ua.edu, [5]mkamrul@crimson.ua.edu

Abstract— **This paper presents a detailed finite-element analysis of the 2012 Nissan Leaf interior permanent-magnet synchronous motor (IPMSM) using conventional rare-earth Nd-Fe-B (N35) and rare-earth-free Fe_2Ni_2N magnets. An electromagnetic model was developed in ANSYS Maxwell to evaluate both magnets under inverter-limited conditions, incorporating Maximum Torque per Ampere (MTPA), Flux-Weakening (FW), and Maximum Torque per Voltage (MTPV) control strategies. Four voltage–current combinations (375 V-480 A, 187 V-480 A, 187 V-240 A, and 375 V-240 A) were simulated to analyze their effects on the torque–speed envelope and efficiency. Results indicate that Fe_2Ni_2N closely matches N35 in terms of torque, flux-weakening, and efficiency performance across all operating regimes. The study confirms that inverter voltage and current variations significantly impact on the torque and efficiency characteristics of the IPMSM. Under these varying conditions, Fe_2Ni_2N maintains performance comparable to N35, reinforcing its potential as a rare-earth-free alternative for traction applications.**

Index Terms **— Fe_2Ni_2N, NdFeB (N35), rare-earth-free permanent magnet, IPMSM, finite-element analysis (FEA)**

I. Introduction

Electric vehicles (EVs) demand traction motors that deliver high torque density, broad constant-power speed range, and high efficiency within tight packaging and thermal constraints. Interior permanent-magnet synchronous machines (IPMSMs) are widely adopted because they combine magnetic and reluctance torque to achieve excellent torque–speed characteristics in compact designs [1], [2]. The 2012 Nissan Leaf IPMSM is often used as a reference platform in benchmarking and laboratory evaluations, making it a practical template for comparative studies of materials and drive limits [3].

IPMSM performance largely depends on rare-earth (RE) permanent magnets (PMs), especially Nd–Fe–B. However, reliance on rare earths introduces supply-chain vulnerability, price instability, and environmental issues noted in international analyses [4]. Despite ongoing research into reduced-rare-earth or magnet-less designs, most alternatives encounter trade-offs in torque density and maximum magnetic energy density [5], [6].

Concurrently, emerging magnet families are being studied to sustain performance while reducing exposure to critical materials.

Recent studies highlight candidates such as ordered FeNi ($L1_0$) and iron-nitride systems for EV drive motors, emphasizing that improved anisotropy and coercivity are prerequisites for replacing Nd-Fe-B in traction applications [7]. Within this field, Fe-Ni-N alloys have drawn attention: theoretical and experimental studies report stable ordered phases and promising intrinsic magnetic properties across Fe–Ni–N compositions, while iron-nitride phases (e.g., α''-$Fe_{16}N_2$) continue to advance in bulk processing and consolidation routes[8], [9], [10].

While advances in magnetic materials continue to drive innovation, PMSM performance relies on the integrated interaction of magnet properties, machine geometry, thermal conditions, and control strategy. Traditional research has focused on improving remanence, coercivity, and magnetic energy density to boost torque and efficiency, while modern control methods such as MTPA, FW and MTPV remain essential for optimal drive operation [11], [12]. However, most studies focus on materials, electromagnetic design, and control separately, overlooking their interdependence.

This work bridges these aspects by evaluating Fe_2Ni_2N substitution in the 2012 Nissan Leaf IPMSM through finite-element analysis under realistic inverter constraints, providing system-level insight into Fe–Ni–N magnets as rare-earth-free alternatives for high-efficiency traction applications.

In this paper, Section II examines the magnetic properties and demagnetization behavior of NdFeB (N35) and Fe_2Ni_2N. Section III details the specifications of the 2012 Nissan Leaf IPMSM in ANSYS Maxwell, while Section IV describes MTPA, Flux-Weakening, and MTPV control strategies that govern torque production. Section V compares the electromagnetic performance of both magnets under various

979-8-3315-8138-1

voltage–current limits, and Section VI concludes that Fe_2Ni_2N achieves performance comparable to N35 under realistic inverter constraints.

II. Magnetic Materials Characteristics

PMSMs partly relies on rotor magnet properties to achieve high torque density, efficiency, and stability under demagnetization of motor armature reaction. The performance depends on the magnet's ability to (1) be magnetized or demagnetized by an external field and (2) retain magnetization after the field is removed. These behaviors are illustrated by the normal and intrinsic B–H hysteresis curves, which define the relationship between magnetic flux density and magnetic field intensity. Fig. 1 shows a typical *B–H* loop (intrinsic and normal), illustrating the temperature-dependent demagnetization curves of Nd-Fe-B magnets.

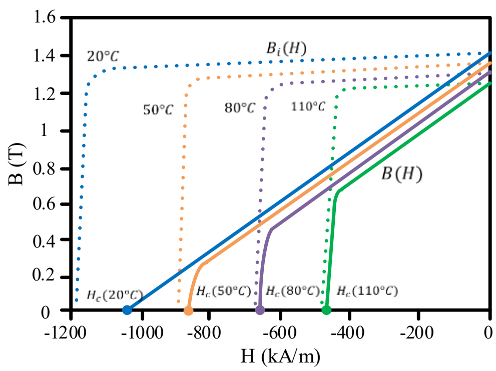

Fig 1. Illustration of intrinsic and normal demagnetization curves in a B–H hysteresis loop for Nd-Fe-B magnet.

At the motor level, temperature changes influences remanence B_r and coercivity H_c, thereby affecting torque and efficiency. Magnet behavior can be modeled using a linear (1) or hyperbolic demagnetization approximation [13]:

$$B = B_r\left(1 - \frac{H}{H_c}\right) \tag{1}$$

This analytical model captures the magnet's gradual loss of magnetic flux under high demagnetizing fields, which is essential for accurate simulation in high-current or flux-weakening conditions. Below, we introduce two permanent magnets used in the motor performance test: one is a rare-earth magnet, and the other is a rare-earth-free magnet.
Table I shows the magnetic properties of the two permanent magnets.

A. *Conventional Rare-Earth Magnet: Nd-Fe-B(N35)*

Nd-Fe-B remains the benchmark for EV traction motors because of its highest maximum magnetic energy density (BH_{max}) and strong magnetic strength. With B_r =1.2 T and H_c = 0.907 MA/m, N35 enables compact, torque-dense designs. However, reliance on rare-earth elements such as Nd and Dy poses supply-chain and environmental risks.

B. *Emerging Rare-Earth-Free Magnet: Fe_2Ni_2N*

Recent advances in ferromagnetic alloys have highlighted FeNi-based compounds as promising rare-earth-free alternatives. The Fe-Ni alloy exhibits high saturation magnetization but suffers from low magnetocrystalline anisotropy energy (MAE ≈ 0.47 MJ/m³), which limits its coercivity for permanent-magnet applications. To overcome this, interstitial nitrogen doping has been introduced, forming iron–nickel nitride (Fe_2Ni_2N) compounds with significantly enhanced anisotropy. This modification increases the magnetocrystalline anisotropy constant (K_u) from 0.47 MJ/m³ for FeNi to approximately 1.94 MJ/m³ for Fe_2Ni_2N [10]

Table I. Remanent and coercivity -for permanent magnets.

Magnet	B_r (*T*)	H_c (MA/m)
NdFeB (N35) [14]	1.2	0.907
MnBi	0.55	1.1
Fe_2Ni_2N [10]	1.2 (Theoretical)	0.957 (Theoretical)
Ferrite (Y32)	0.4	0.27

C. *Demagnetization Characteristics*

The demagnetization curves of NdFeB (N35) and Fe_2Ni_2N along with other permanent magnet's (PM's) such as MnBi, Ferrite, are compared in Fig 2, derived from their respective B–H characteristics, summarized in Table I. Both N35 and Fe_2Ni_2N materials exhibit nearly identical remanent flux density. However, Fe_2Ni_2N shows slightly higher resistance to demagnetization.

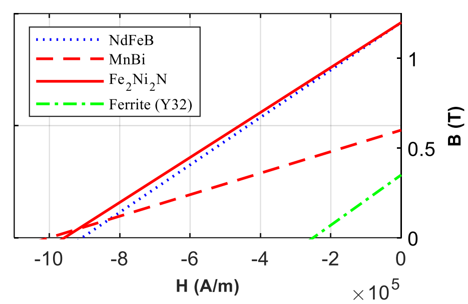

Fig 2. Demagnetization curves for the relevant PM.

Thus, Fe_2Ni_2N achieves a balance of rare-earth independence, competitive remanence, and greatly enhanced coercivity, making it as a strong contender for next-generation PMSMs. Its potential for easy replacement within existing motor geometries, such as the 2012 Nissan Leaf IPMSM, will be thoroughly assessed through finite-element analysis in the following sections.

D. *Influence of coercivity and (BH)max*

The magnetic properties of a permanent magnet, especially coercivity (H_c) and $(BH)_{max}$, greatly influence PMSM performance. Coercivity represents resistance to demagnetization, while $(BH)_{max}$ determines magnetic energy density. When the stator field $H_m(i_d, i_q)$ increases, the magnet's operating point shifts along the *B–H* curve (Fig. 3), reducing flux linkage, especially in flux-weakening regions. The relation can be expressed as [13]:

$$B_m(i_d, i_q) = B_r\left(1 - \frac{H_m(i_d, i_q)}{H_c}\right), \tag{2}$$

979-8-3315-8138-1

where B_r is the remanent flux density. A higher $(BH)_{max}$ results in a smaller magnet volume and higher power density, while its lower values require larger magnets or stronger excitation.

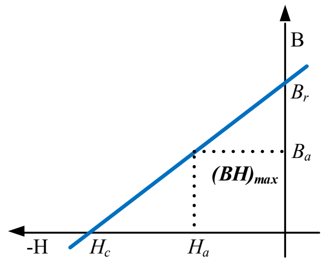

Fig 3. Demagnetization normal curve (2nd quadrant).

As shown in Fig. 4, the knee point of the demagnetization curve marks the onset of irreversible loss; magnets with higher H_c maintain stability farther from this region.

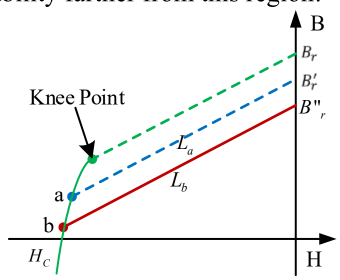

Fig 4. Illustration of the knee point and irreversible demagnetization.

Understanding these magnetic properties is crucial for accurately modeling motor performance. The following section describes the finite-element modeling and simulation framework of the 2012 Nissan Leaf IPMSM, used to assess both the impact of inverter voltage–current variations and the comparative performance of Fe_2Ni_2N and N35 magnets under the same operating conditions.

TABLE II. 2012 NISSAN LEAF SPECIFICATION.

Parameter	Value	Unit
Slot Number	48	-
Pole Number	8	-
Stator Bore (mm)	132	mm
Rotor Diameter (mm)	130	mm
Airgap (mm)	1	mm
Shaft Diameter (mm)	40	mm
Axial length	260	mm
Phases	3	3

III. DESIGN SPECIFICATIONS OF THE NISSAN LEAF

The 2012 Nissan Leaf IPMSM is chosen as the benchmark because of its validated geometry, available open data broad previous use in EV motor research. A FEA model was developed in ANSYS Maxwell to replicate the machine's electromagnetic behavior. The machine uses an interior V-shaped magnet topology embedded within the rotor to achieve magnetic saliency and combine magnet and reluctance torque production. Key design parameters are summarized in Table II, and the corresponding motor geometry is shown in Fig. 5.

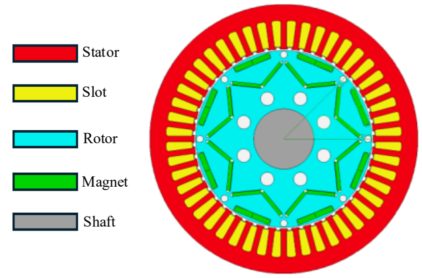

Fig 5. Structure of the Nissan Leaf IPMSM.

IV. IPMSM CONTROL: MTPA, FLUX WEAKENING, AND MTPV

Accurate assessment of motor performance needs modeling both the magnetic properties of the rotor materials and the inverter's voltage–current constraints that affect torque and efficiency throughout the entire operating range. The IPMSM torque-control strategy regulates electromagnetic torque T_{em} and flux linkages λ_d, λ_q within inverter voltage and current constraints while maximizing efficiency. The control of the motor torque T_{em} is achieved through d- and q-axis current components of the motor, the i_d^* and i_q^*, which generate voltage control commands v_d^* and v_q^*, that are applied to the motor inverter through space-vector PWM. The PMSM voltage Eq. (3) in the rotor-aligned dq frame is expressed as [31]:

$$\begin{bmatrix} v_d \\ v_q \end{bmatrix} = R \begin{bmatrix} i_d \\ i_q \end{bmatrix} + \frac{d}{dt} \begin{bmatrix} \lambda_d \\ \lambda_q \end{bmatrix} + \omega_e \begin{bmatrix} -\lambda_q \\ \lambda_d \end{bmatrix}. \quad (3)$$

The overall operation regions are shown in Fig. 6, where the current- and voltage-limit ellipses outline three control regions: MTPA, FW, and MTPV. These regimes govern how the current vector changes as speed and back-EMF increase, ensuring wide constant-power operation and torque stability.

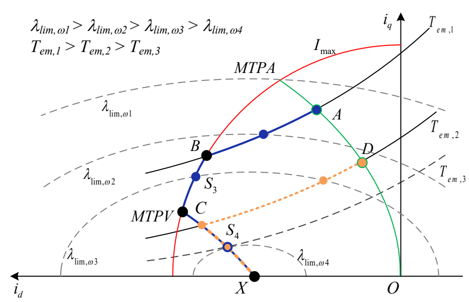

Fig 6. From torque to current references, considering current and voltage limits.

A. *Maximum Torque per Ampere (MTPA)*

In the low-speed region (inner trajectory of Fig. 6), the current magnitude is minimized for a given torque while staying within inverter voltage limits. The MTPA strategy regulates the stator current vector (i_s) so that maximum torque per unit current is achieved before entering the flux-weakening region. The optimization can be expressed as:

$$\text{minimize } |i_s| = \sqrt{i_d^2 + i_q^2}$$

$$\text{subject to } T_{em}^* = \frac{P}{2}\left(\lambda_{pm} i_q + \left(L_d - L_q\right) i_d i_q\right),$$

where p is the pole-pair number, L_d and L_q are the d- and q-axis stator inductances, respectively. This formulation ensures maximum torque per unit before reaching the flux-weakening region, providing efficient torque production and optimal current utilization up to the base speed.

B. Flux Weakening (FW)-I

As the motor speed increases and the back-EMF approaches the inverter voltage boundary (transition A → B in Fig. 6), a negative i_d component is introduced to counteract the magnetic flux. The current vector is adjusted to sustain commanded torque while staying within voltage constraints, as described by

$$\text{minimize } |i_s| = \sqrt{i_d^2 + i_q^2}$$

$$\text{subject to } T_{em}^* = \frac{P}{2}\left(\lambda_{df} i_q + \left(L_d - L_q\right) i_d i_q\right)$$

$$\sqrt{\left(L_d i_d + \lambda_{pm}\right)^2 + \left(L_q i_q\right)^2} \le \lambda_{\lim,\omega_e}.$$

Here, λ_{pm} denotes the magnet flux linkage. This flux-weakening action extends the constant-power region without surpassing the inverter's voltage capability.

C. Flux Weakening (FW)-II

Beyond point B (region B → C in Fig. 6), both voltage and current limits become active. The controller minimizes torque deviation while maintaining the stator current near its rated magnitude to prevent excessive demagnetizing fields:

$$\left|T_{em}^* - T_{em,lim}\right| = min,\ \ i_d^2 + i_q^2 = i_{rated}^2$$

where $T_{em,\,lim}$ represents the torque corresponding to the flux-weakening limit. This ensures smooth torque transition, magnetic stability, and sustained efficiency during deep flux-weakening operation.

D. Maximum Torque per Voltage (MTPV)

At extreme high-speed operation (outer boundary C → X in Fig. 6), the IPMSM reaches simultaneous current–voltage saturation. The MTPV strategy aligns the voltage vector tangentially to the voltage-limit ellipse, maximizing the achievable torque under full inverter utilization:

$$|V| = V_{max},\ \ \frac{dT_{em}}{di_q} = 0$$

where $|V|$ is the stator voltage vector magnitude and $V_{\max}$ is the inverter's maximum allowable voltage amplitude. This condition guarantees maximum torque extraction while maintaining stable operation in the high-speed region.

The established control framework facilitates evaluation of how magnetic material choice influences electromagnetic performance under inverter constraints. Section V presents finite-element results comparing Fe_2Ni_2N and N35 magnets across four operating scenarios, highlighting how voltage current limits shape torque–speed and efficiency.

V. Comparative Electromagnetic Performance Analysis: N35 versus Fe_2Ni_2N

To assess how magnet substitution affects traction performance, finite-element electromagnetic simulations were conducted on the 2012 Nissan Leaf IPMSM, which uses either NdFeB (N35) or Fe_2Ni_2N as rotor magnets.

All simulations used the same geometry, boundary conditions, and control algorithms (MTPA, flux-weakening, and MTPV) as described in Sections III and IV. Four inverter-limited operating scenarios were examined to reflect realistic drive conditions: (1) 375 V–480 A, (2) 187 V–480 A, (3) 187 V–240 A, and (4) 375 V–240 A. Each case provides insight into the combined effect of voltage and current constraints on torque and efficiency when using different magnet materials.

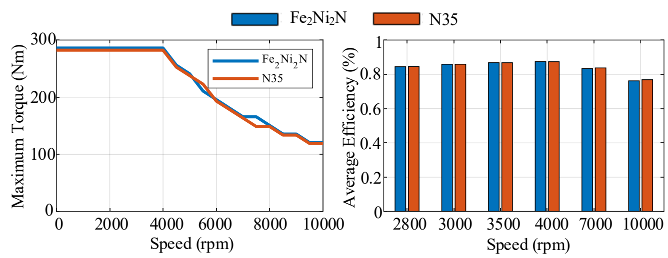

Fig 7. Maximum average torque and efficiency of Nissan Leaf at 375V dc bus voltage and 480A peak current.

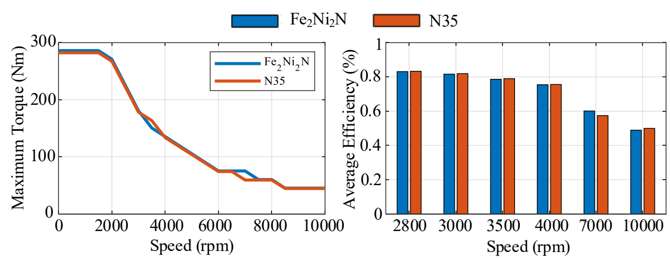

Fig 8. Maximum average torque and efficiency of Nissan Leaf at 187V dc bus voltage and 480A peak current.

A. Case 1: High Voltage and High Current

Under rated voltage and current, both N35 and Fe_2Ni_2N produce nearly identical torque–speed profiles (Fig. 7). The peak torque reaches approximately 282 N·m, with a gradual decrease in the flux-weakening region as the back-EMF approaches the inverter limit. The constant torque zone extends up to around 4000 rpm, then decreases linearly toward 10,000 rpm. The efficiency curve for both magnets exceeds 80% in the base-speed region. The results confirm that Fe_2Ni_2N performs comparably to N35 under nominal drive conditions, indicating that magnetic substitution has little effect on overall capability.

B. Case 2: Low Voltage and High Current

At a lower DC bus voltage, the inverter's voltage limit restricts the back-EMF magnitude, thereby reducing the maximum torque achievable within the constant-torque region. As shown in Fig 8, both magnetic materials exhibit the same peak torque of about 282 N.m, and the reduced constant-torque region contracts to approximately 2000 rpm. The efficiency stays near 80% throughout most of the mid-speed range. This

979-8-3315-8138-1

case shows that voltage reduction mainly affects the speed range, and both magnets have identical control transitions between MTPA and flux-weakening regions.

C. Case 3: Low Voltage and Low Current

When both the voltage and current limits are constrained (Fig. 9), the motor runs under the most restrictive condition. The peak torque drops to approximately 150 N·m. Both N35 and Fe_2Ni_2N follow comparable torque–speed trajectories, indicating that torque capacity is primarily governed by electrical boundary conditions.

D. Case 4: High Voltage and Low Current

At rated voltage but reduced current (Fig. 10), both magnets achieve similar maximum torque (~150 N·m) and identical torque roll-off patterns. The efficiency profile remains steady above 80%, indicating that reduced current mainly affects torque magnitude, while high voltage further extends the constant torque region. This further demonstrates that both Fe_2Ni_2N and N35 maintain similar electromagnetic performance under current-constrained operation.

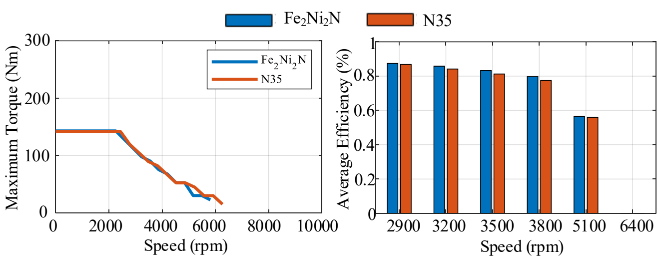

Fig 9. Maximum average torque and efficiency of Nissan Leaf at 187V dc bus voltage and 240A peak current.

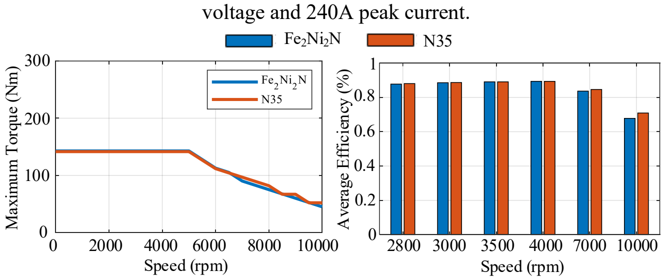

Fig 10. Maximum average torque and efficiency of Nissan Leaf at 375V dc bus voltage and 240A peak current.

Fe_2Ni_2N and N35 show nearly identical torque–speed and efficiency characteristics across all test conditions, confirming Fe_2Ni_2N as a viable rare-earth-free alternative for IPMSM drives. Variations in voltage–current limits indicate that inverter constraints, not magnet type, control torque and power behavior. Both magnets provide similar performance over the entire operating range, with Fe_2Ni_2N offering the benefit of being rare-earth-free magnet.

VI. Conclusion

This study conducted a comparative finite-element analysis of the 2012 Nissan Leaf IPMSM using NdFeB (N35) and Fe_2Ni_2N rotor magnets to assess the feasibility of rare-earth-free design under different inverter voltage-current conditions. A unified modeling and control framework incorporating MTPA, flux-weakening, and MTPV strategies was applied under four inverter-limited conditions (375 V–480 A, 187 V–480 A, 187 V–240 A, and 375 V–240 A). Results demonstrate that Fe_2Ni_2N attains torque–speed and efficiency performance comparable to N35, with both magnets reaching similar peak torque (≈282 N·m) and efficiency levels. The analysis further shows that inverter voltage–current fluctuations primarily influence performance supporting Fe_2Ni_2N's potential as a sustainable, rare-earth-free alternative for EV traction applications without losing torque or drive efficiency.

Acknowledgment

This research was partly funded by the National Science Foundation through award numbers IUCRC 2137275 and RAISE-CET 2402634.

References

[1] J.-M. Mun, G.-J. Park, S. Seo, D.-W. kim, Y.-J. Kim, and S.-Y. Jung, "Design Characteristics of IPMSM With Wide Constant Power Speed Range for EV Traction," *IEEE Transactions on Magnetics*, vol. 53, no. 6, pp. 1–4, Jun. 2017, doi: 10.1109/TMAG.2017.2664859.

[2] S. Guo, X. Su, and H. Zhao, "Optimal Design of an Interior Permanent Magnet Synchronous Motor for Electric Vehicle Applications Using a Machine Learning-Based Surrogate Model," *Energies*, vol. 17, no. 16, p. 3864, Jan. 2024, doi: 10.3390/en17163864.

[3] T. Burress and S. Campbell, "Benchmarking EV and HEV power electronics and electric machines," in *2013 IEEE Transportation Electrification Conference and Expo (ITEC)*, Jun. 2013, pp. 1–6. doi: 10.1109/ITEC.2013.6574498.

[4] International Energy Agency, *Critical Minerals Market Review 2023*. OECD, 2023. doi: 10.1787/9cdf8f39-en.

[5] M. Kimiabeigi *et al.*, "High-Performance Low-Cost Electric Motor for Electric Vehicles Using Ferrite Magnets," *IEEE Transactions on Industrial Electronics*, vol. 63, no. 1, pp. 113–122, Jan. 2016, doi: 10.1109/TIE.2015.2472517.

[6] B. Podmiljšak *et al.*, "The Future of Permanent-Magnet-Based Electric Motors: How Will Rare Earths Affect Electrification?," *Materials (Basel)*, vol. 17, no. 4, p. 848, Feb. 2024, doi: 10.3390/ma17040848.

[7] C. L. Rom, R. W. Smaha, S. O'Donnell, S. Dugu, and S. R. Bauers, "Emerging magnetic materials for electric vehicle drive motors," *MRS Bulletin*, vol. 49, no. 7, pp. 738–750, Jul. 2024, doi: 10.1557/s43577-024-00743-4.

[8] T. Saito, H. Yamamoto, and D. Nishio-Hamane, "Production of Rare-Earth-Free Iron Nitride Magnets (α″-Fe16N2)," *Metals*, vol. 14, no. 6, p. 734, Jun. 2024, doi: 10.3390/met14060734.

[9] D. Tuvshin, T. Tsevelmaa, S. C. Hong, and D. Odkhuu, "Fe–Ni–N based alloys as rare-earth free high-performance permanent magnet across α''phase transition: A theoretical insight," *Acta Materialia*, vol. 210, p. 116807, May 2021, doi: 10.1016/j.actamat.2021.116807.

[10] M. A. Wahed *et al.*, "Quantum mechanical design of rare-earth-free ferromagnetic material incorporating 2*p* element doping for permanent magnet applications," *Journal of Magnetism and Magnetic Materials*, vol. 615, p. 172775, Mar. 2025, doi: 10.1016/j.jmmm.2025.172775.

[11] S. Huang, Z. Chen, K. Huang, and J. Gao, "Maximum torque per ampere and flux-weakening control for PMSM based on curve fitting," in *2010 IEEE Vehicle Power and Propulsion Conference*, Sep. 2010, pp. 1–5. doi: 10.1109/VPPC.2010.5729024.

[12] N. Bianchi, P. G. Carlet, L. Cinti, and L. Ortombina, "A Review about Flux-Weakening Operating Limits and Control Techniques for Synchronous Motor Drives," *Energies*, vol. 15, no. 5, p. 1930, Jan. 2022, doi: 10.3390/en15051930.

[13] J. F. Gieras, *Permanent Magnet Motor Technology: Design and Applications, Third Edition*, 3rd ed. Boca Raton: CRC Press, 2009.

[14] "Neodymium Magnets (NdFeB)," Arnold Magnetic Technologies. Accessed: Nov. 03, 2025. [Online]. Available: https://www.arnoldmagnetics.com/products/neodymium-iron-boron-magnets/

979-8-3315-8138-1